JOURNAL OF SPACECRAFT AND ROCKETS
Vol. 46, No. 3, May–June 2009

Ground Effects for Widely Spaced, Supersonic, Vertical Retrorockets

Richard E. Wirz*
University of California, Los Angeles, Los Angeles, California 90095
and
Shaun S. Shariff†
Metacomp Technologies Inc., Agoura Hills, California 91301

DOI: 10.2514/1.36299

A scenario for creating acceptable touchdown velocity on land for the Orion Crew Excursion Vehicle employs retrorockets for final landing ΔV. To capture the ground effects due to the interaction of the retrorockets and the vehicle, detailed computational modeling was used to determine the effective thrust at several different firing heights. These results were then used to determine the change in impulse for a wide range of possible firing altitudes. For a Crew Excursion Vehicle retrorocket firing time of 0.5 s, the steady-state effective vertical thrust of the module changes from −13.2 to +11.8% for altitudes from 152 to 15.2 cm, respectively. A simple descent analysis shows that ground effects will impart a net decrease or increase in impulse, depending on ignition altitude. In this analysis, the ground effects serve to increase the optimal firing height and increase the ignition altitude margin for a given maximum landing velocity.

Nomenclature

a = acceleration, m/s^2
h = altitude, m
M = Mach number
P = pressure, N
v = velocity, m/s

I. Introduction

VERTICAL retrorockets, in conjunction with parachutes, are an option for minimizing the landing velocity of NASA's Orion Crew Excursion Vehicle (CEV) for ground-based landings. For this scenario, CEV will deploy a parachute after reentry to slow its vertical velocity to about 7 m/s, after which the vertical retrorockets will fire for ∼0.5 s to further slow the vertical velocity to less than 1 m/s immediately before touchdown. For this scenario, it is important to understand how the interaction of the rockets with the ground surface and vehicle body will change the effect thrust and ΔV imparted by the retrorockets. As discussed in the following section, ground effects are relatively well understood for vertical aircraft propellers but are not well understood for the widely spaced retrorocket configuration for CEV.

In this study, we investigate the ground effects for widely spaced supersonic retrorockets fixed on a relatively large descending body using computational modeling. The configuration used herein reflects the current retrorocket design for CEV. Analysis at several firing heights and a groundless condition are used to determine the variation of effective thrust due to ground effects for various firing altitudes. These results are then used to develop descent profiles for various ignition altitudes to assess the impact of ground effects on the final phase of CEV descent.

The Apollo program investigated retrorockets for both water and ground landings [1]. Results from the Apollo land drop tests with retrorockets revealed an initial loss in thrust during the early part of thruster firing, followed by a gain in thrust due to ground effects. Figure 1 shows the deviations from the expected thrust profile, showing the effective thrust loss and thrust gain for the Apollo land drop test. In this paper, we discuss the sources of these deviations and how they may manifest for a retrorocket landing of CEV.

Several previous authors have investigated the forces and flowfields due to ground effects for vertical/short takeoff and landing (V/STOL) vehicles using propeller flowfields in the presence of aircraft bodies. Kuhn [2] summarizes most of the analytical and experimental investigations for subsonic multijet flows conducted before 1986. More recent efforts have also investigated the effects of closely spaced supersonic jets several exit diameters from flat surfaces [3–5]. These previous efforts do not capture the unique flows created by CEV, for which we must examine the flowfield for widely spaced supersonic jets over a wide range of firing altitudes. The CEV retrorocket firing case also requires analysis of a large, relatively flat, base surface near the ground; the differential pressure forces acting over this large surface can have a significant impact on effective thrust. To do this unique analysis, we combine detailed computational modeling of the retrorockets' plume interaction with the ground and CEV underside at several firing heights to determine the effective change in thrust due to proximity to the ground. We isolate the ground effects, which has not been done in previous studies, by comparing these results with the effective change in thrust due to the local flowfield induced by the retrorocket firing without the presence of the ground. These results are used in an analytical model to determine the effective change in impulse due to ground effects for a range of possible firing heights for CEV retrorocket landing scenarios.

Before getting into the details of the analysis, the following discussion is provided to introduce the reader to the terminology that we use in this paper to discuss the various elements of ground effects. When appropriate, we adopt terminology used in previous studies, for consistency. In this paper, we call an effective loss in the total thrust a *thrust loss* (termed the *suckdown force* in some previous literature) and an effective gain in thrust is called *thrust gain*. For a single-jet flow or a multijet flow without a nearby impinging surface, thrust loss is caused by a pressure decrease along the underside of the landing craft, due to entrainment of the local air by the turbulent shear layer

Presented as Paper 5758 at the 43rd AIAA/ASME/SAE/ASEE Joint Propulsion Conference, Cincinnati, OH, 8–11 July 2007; received 21 April 2008; revision received 19 October 2008; accepted for publication 19 October 2008.

*Assistant Professor, Department of Mechanical and Aerospace Engineering; wirz@ucla.edu.
†Scientist, 28632-B Roadside Drive, Suite 255.

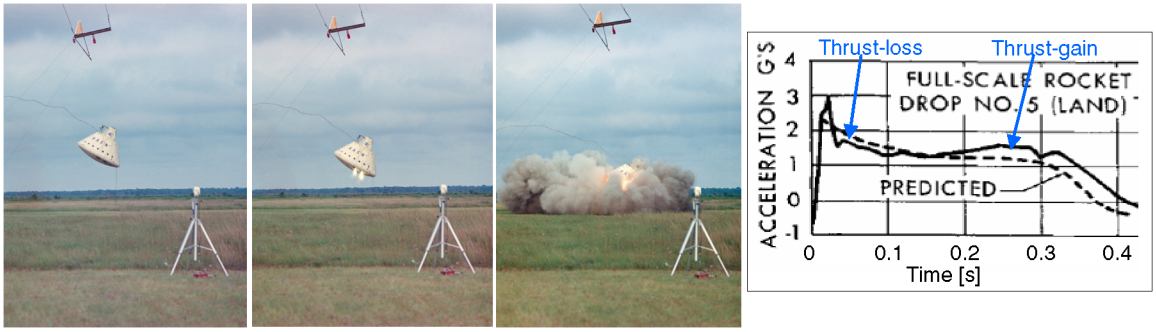

Fig. 1 Apollo land drop-test images and data from [1].

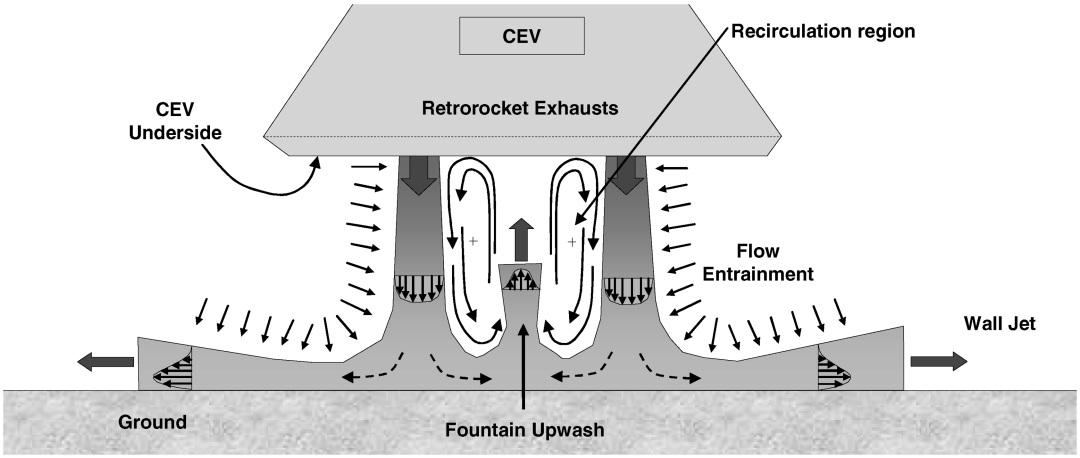

Fig. 2 Schematic of the retrorocket flowfield near the ground.

along the edge of the thruster plume(s). For a single-jet flow, the presence of a nearby surface, such as the ground, can increase thrust loss because the wall jets, created by the ground turning the flow, can effectively increase the area of the plumes' turbulent shear layer and thus increase the flow entrainment near the vehicle underside [5]. This effect also exists for multijet flows, but as shown in Fig. 2 (inspired by diagrams from [2,4]), recirculation regions can arise that can further decrease the loss of pressure on the vehicle underside along much of the vehicle underside. However, in the multithruster configuration, the fountain upwash between the plumes causes an increase in pressure on the vehicle underside that, for most altitudes, partially offsets the suction force of the thrust loss [6]. At lower altitudes, this fountain upwash can become more significant than the thrust-loss effects, thus causing the total pressure integrated over the underside to increase beyond ambient pressure, with the effects resulting in a total thrust gain. This thrust gain caused by fountain upwash is typically referred to as the *ground effects*; however, the additional thrust-loss effects due to the ground is a ground effect as well.

II. Computational Investigation of Ground Effects for CEV

In this section, we use steady-state CFD solutions to provide an assessment of ground effects for CEV during vertical retrorocket firing that occurs immediately before touchdown. The steady-state results are used to determine how the ground effects will alter the vehicle descent during retrorocket fining. These phenomenological results are intended to guide future modeling efforts that will include detailed transient analyses.

A. Steady-State Computational Analysis of Ground Effects for CEV

The retrorocket landing configuration for CEV employs four vertically oriented solid rocket motors (SRMs), as shown in Fig. 3. This configuration used in this study assumes that the heat shield has been dropped well before the final descent phase when the vertical rockets are fired. The mass of the vehicle without the heat shield is approximately 7200 kg and the moment of inertia about the y axis is approximately $21,000\ \text{kg} \cdot \text{m}^2$. The total thrust from the four thrusters totals approximately 178 kN, and the forward SRMs (on the negative z side) provide 30% more thrust to achieve thrust centered with the module c.g., which is several inches off the body axis in the negative z direction. The exit conditions for both rocket sets are assumed to be identical, perfectly expanded, with an assumed exit Mach number of $M = 4.09$. For the current CEV design, the SRMs fire for 0.5 s before the touchdown and are designed to provide approximately 2–2.5 g of deceleration. The maximum diameter of the vehicle is 5 m. As shown in Fig. 3, the x–z plane is the plane of symmetry used in the computational model and the body's axis (i.e., the x axis) is antivertical.

To estimate the ground effects for CEV, we modeled the multiplume flow using CFD++ from Metacomp Technologies, Inc. [7]. CFD++ uses a discretization based on multidimensional polynomials and the Harten–Lax–van Leer type C approximate Riemann solver [8]. The multidimensional polynomials preserve linearity, meaning that they represent linear variations exactly on arbitrary grids. This methodology leads to low levels of numerical dissipation. It has been applied to many benchmark calculations, including the AIAA Drag Prediction Workshops. The first Drag Prediction Workshop (DPW) involved predicting the drag polar for a wing/fuselage combination. DPW II involved the same combination and another computation in which a pylon and nacelle were added to the wing. CFD++ demonstrated good comparison of the drag polar with experimental results. CFD++ was one of the few codes that demonstrated consistency under grid refinement, meaning that as the grid was refined, the solution compared even better with the experimental data. However, good results were achieved even on coarse grids.[‡]

[‡]Data available online at http://aaac.larc.nasa.gov/tsab/cfdlarc/aiaa-dpw/ [retrieved 23 February 2009].

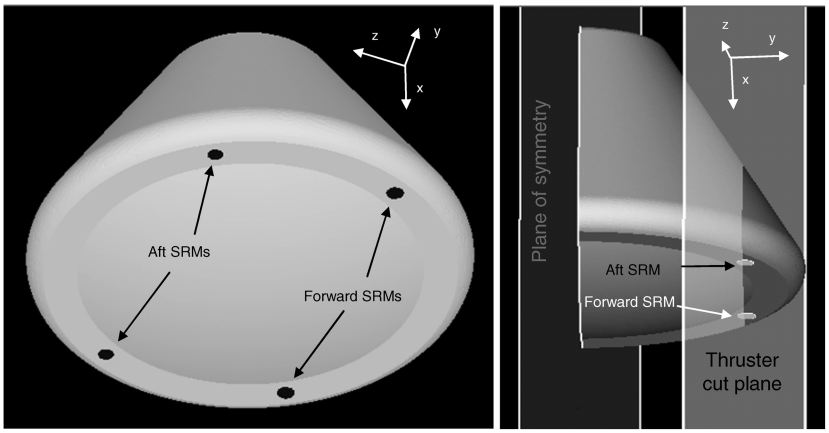

Fig. 3 Vertical retrorocket configuration on CEV and computational domain.

The solutions presented here were computed using the compressible perfect-gas equations in conjunction with the k-ε-R_t turbulence model. The k-ε-R_t turbulence model (recently submitted for publication) combines the effects of Metacomp's realizable k-ε model with Metacomp's R_t model. Both models are good at resolving effects due to free shear and wall shear, but the R_t model is better at preserving core turbulence levels in regions of low shear and is preferable because most two-equation models cannot preserve the core turbulence as the flow moves from regions of fine grid (as in the jets) to coarser regions (between the jets and away from the body). Therefore, this feature allows for better convergence for the mesh structures used in this effort, and in previous similar efforts, this feature has resulted in better agreement with experiment using a grid with a smaller cell count. The function of the turbulence models is to predict a statistically steady-state flow by modeling the turbulent fluctuations. However, in the case of the type of large-scale unsteadiness seen in these problems, a true steady state is not possible, even with turbulence models. Wall functions were used in conjunction to model the boundary layer so that a coarser grid could be used (rather than resolving the boundary layers with smaller near-wall cells). Wall functions are based on the turbulence model and result in a very good prediction of fluxes at the wall, and they take into account compressibility, heat transfer, and pressure gradient. A wall function is an accurate description of near-wall turbulence for fully

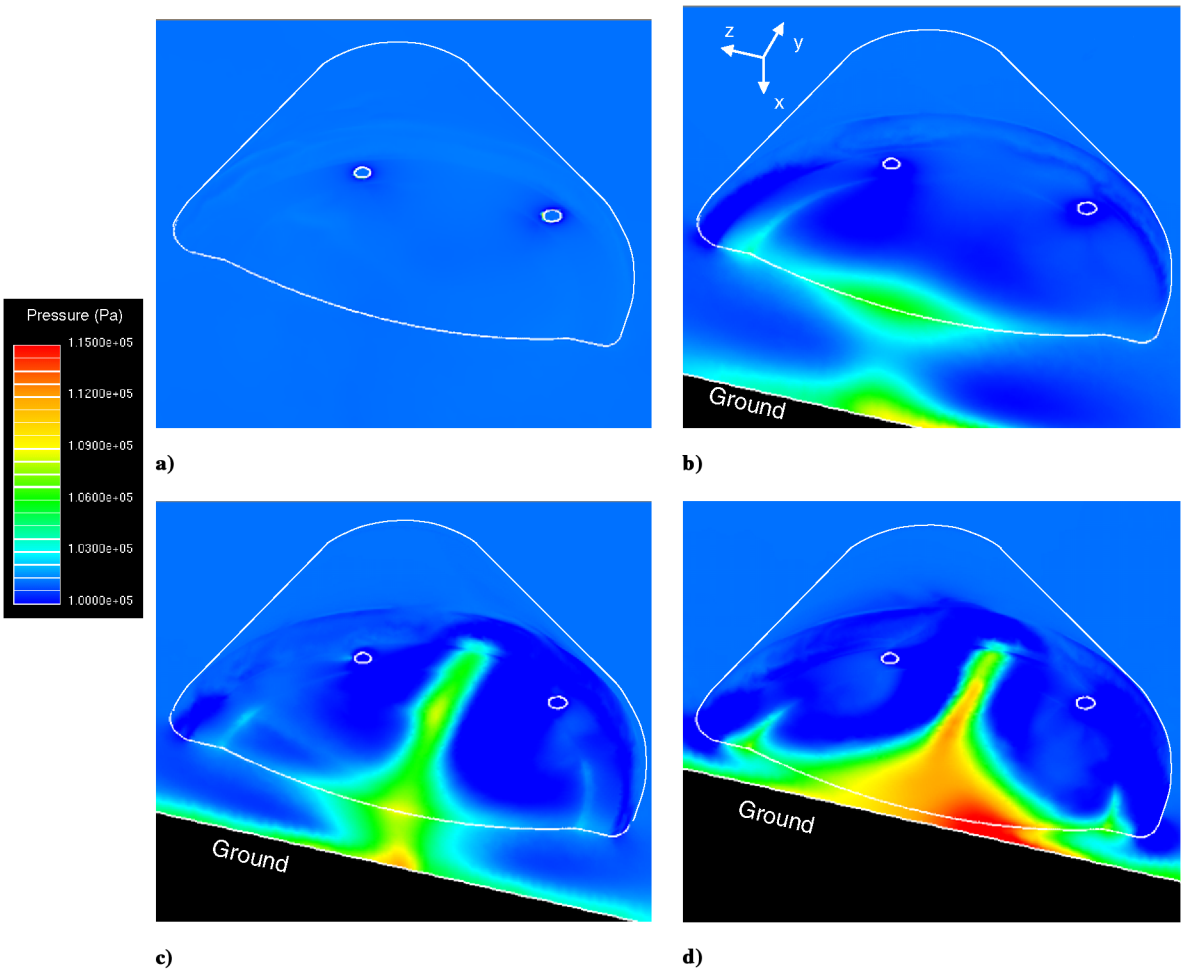

Fig. 4 Pressure distribution on CEV during vertical retrorocket firing at different altitudes h with a) $h = \infty$, b) $h = 152$ cm, c) $h = 76$ cm, and d) $h = 15.2$ cm ($P_{\text{atm}} = 1.013\text{e} + 05$ Pa).

developed flat-plate flow and flows across curved surfaces with relatively large radii of curvature. It bridges the gap between the wall and the logarithmic overlap layer, thereby allowing coarser grids and shorter run times. Deviations from flat-plate flow are taken into account by varying the baseline law of the wall. The walls (i.e., the vehicle and the ground) were assumed to be adiabatic.

The grids for the simulations ranged between 3.9 million and 4.9 million cells for the cases in which the ground was present and up to 10.5 million cells for the cases with no ground. The bulk of the cells are in the region around and between the jets. Very fine cells are needed to properly resolve the shear layers around the jets; therefore, more cells were required for the no-ground cases, because the jets extend much farther without the ground. The grids consisted of tetrahedra with triangular prisms to resolve the boundary layer (or triangles and quadrilaterals for the axisymmetric runs). Grid refinement studies were performed in the early stages of this investigation to assess the adequacy of the grid to resolve salient fluid dynamic features. Early grids insufficiently resolved the shear layers, and so the grid was refined in the region of the jets, allowing the turbulence model to properly model the correct eddy viscosity. Subsequent refinement of the grid did not change the results significantly. This approach was used with the later grids as well.

For this preliminary analysis, we obtain steady-state solutions with the thrusters firing at altitudes h of infinity, 152 cm (60 in.), 76 cm (30 in.), and 15.2 cm (6 in.). Each of these cases is compared against the assumption that when ground effects are ignored, the pressure across the vehicle surface is assumed to be constant and equal to the ambient pressure P_{atm}, which would result in no perceived thrust loss or gain. The $h = \infty$ case is for heuristic purposes, and the three altitudes are indicative of what will be encountered during a typical CEV descent. For the $h = \infty$ case, shown in Fig. 4a, the pressure difference between the underside and top of the body results in a −9.0% thrust loss. For this case, the pressure drop on the underside manifests primarily near the thruster exits, as one would expect for an undisturbed plume flow. As shown in Fig. 4b, the ground at the 152 cm altitude significantly affects the pressure field by increasing the magnitude and area of low pressure while increasing the local pressure near the center and along the z axis of the spacecraft underside. At this altitude, the entrainment effects dominate and the net effect is a −13.2% thrust loss. Similarly, at an altitude of 76 cm (Fig. 4c), the low-pressure regions dominate, causing a thrust loss of −11.2%; however, we began to see the increasing effects of increased pressure on the underside due to fountain upwash. At a firing height of only 15.2 cm (Fig. 4d), the pressure drops along much of the underside, but the pressure increase due to the fountain upwash clearly dominates, resulting in a thrust gain of +11.8%. The torque on CEV due to the pressure distributions shown in Figs. 4b–4d are −7680, −8180, and −1290 Nm about the y axis of the vehicle c.g., respectively. In summary, the results in Fig. 4 show that the integrated body pressure differences result in effective thrust loss of −9.0%, −13.2%, and −11.2% and thruster gain of +11.8%. The impact of the thrust loss/gain and torque on CEV descent is discussed in the next section.

By analyzing the flowfields for the situations in Fig. 4, we can see the interaction of the plumes with the ground. Figure 5 shows streamlines from the nozzle exits, colored per local static pressure. The plume below the nozzle exit is straight because the thrusters nozzle flow is assumed to be perfectly expanded. From these visualizations, we see that the pressure increase on the underside is due to the fountain upwash, which arises from the turning of the jets by the ground and the colliding wall jets between the rocket plumes. Figures 5c and 5d show the expected pressure in the recirculation regions, in which the pressure is high near the stagnation point at the top of the fountain upwash and lower away from the point at which the flow velocity can increase to several hundred meters per second. We can visualize the fountain upwash and entrainment effects if we view the flow along the thruster cut plane from Fig. 3. The unit velocity vectors in Fig. 6 show how the plumes, ground, and body

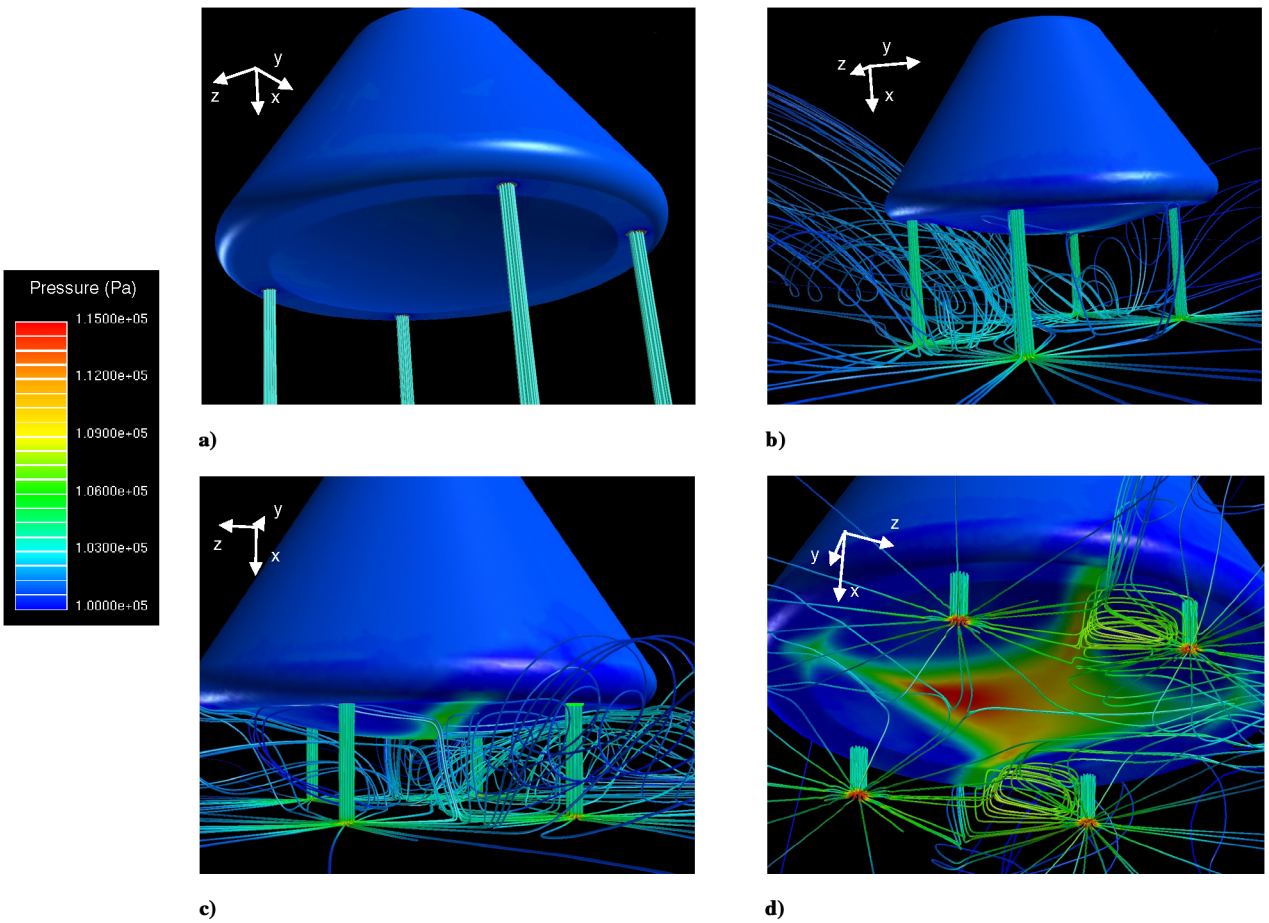

Fig. 5 Visualizations of the plume flowfield for a) no ground, b) altitude = 152 cm, c) altitude = 76 cm, and d) altitude = 15.2 cm.

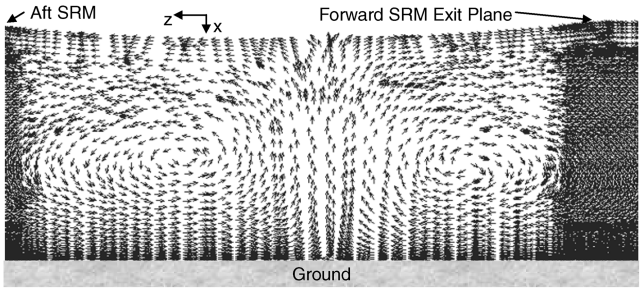

Fig. 6 Unit velocity vectors between rockets on the thruster cut plane (Fig. 3) for altitude = 15.2 cm.

interact to cause a fountain upwash and recirculation region between the jets.

B. Impact of Ground Effects on Vehicle Descent

The steady-state results in the previous section are intended to understand the phenomenon of ground effects and to provide insight for the inputs to a full CFD transient analysis that will be performed in future analyses. For this analysis, these steady-state results provide a reasonable estimate of the thrust loss and gain, because the local velocities of the flow along the vehicle surface due to the thrusters are far greater than the local flow velocities around the body, due to the vehicle descent velocities. In this section, we interpolate and extrapolate these results to perform a simple first-order analysis of the ground effects on CEV descent. These results are preliminary and are not intended to replace the full transient analysis necessary to understand this problem. The ground effects from the results in Fig. 4 are summarized in Fig. 7. To assess the importance of ground effects

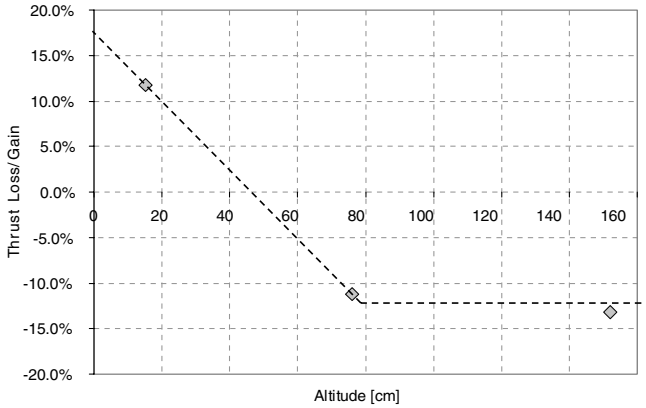

Fig. 7 Percent change in effective thrust as a function of altitude with linear fit.

to first order, we use these data with a simple time-step algorithm for a falling body. The best fit for these data is likely an exponential-type curve; however, to avoid large sensitivities at the lowest altitudes, we assumed the straight-line fits shown in Fig. 7. Future analyses will include full transient analyses; however, because such runs take extremely long run times, this analysis was conducted to qualitatively investigate ground effects. We neglect drag because axisymmetric predictions with CFD + + showed that the drag on the spacecraft is less than 0.5% of the thrust for the maximum final descent velocities (∼7 m/s) for CEV.

For our first-order analysis, we compare CEV descent for cases with ground effects (per Fig. 7) and without ground effects. We assume the approximate CEV retrorocket descent parameters of initial vertical velocity ≅6.68 m/s (toward the ground) and thrusters designed to fire for 0.5 s and provide ∼2.5 g of upward force. The resulting CEV trajectory and corresponding velocity and acceleration for an ignition altitude ∼1.74 m are shown in Fig. 8. For clarity, the acceleration in Fig. 8 is shown at an opposite sign to that of the chosen coordinate system (i.e., x axis pointing toward the ground). For this ignition altitude, the landing velocity is 1.1 m/s with ground effects and 2.0 m/s without. For this case, we see that the vehicle experiences a similar modification to the vehicles acceleration profile by ground effects as was seen during the Apollo land drop test. However, this case results in a 1.7% increase in impulse, whereas the Apollo drop test observed a 7% increase in impulse. These discrepancy may be due to the different configurations or the linear approximations of the data in Fig. 7. Following the altitude and velocity curves of Fig. 8, we can see that for the case in which we include ground effects, the vehicle is at a very low altitude between 0.4–0.5 s, during which it briefly attains an upward velocity and then free falls to the ground. Data from Lands [1] suggest that the Apollo land-based drop experienced a similar trajectory. If we change the ignition height to 2.20 m, we obtain the results shown in Fig. 9, in which we see that thrust gain due to ground effects are minimal, which results in a landing velocity of 2.5 m/s (3.4 m/s without ground effects) and 6.1% loss in total impulse. This loss in total impulse arises from that fact that the rockets terminate firing well before the lowest altitudes at which ground effects provide lift gain. For clarity, the acceleration in Fig. 9 is shown at an opposite sign to that of the chosen coordinate system (i.e., x axis pointing toward the ground).

Using the preceding analysis iteratively, we compare the landing velocity for a wide range of ignition altitudes. For the comparison in Fig. 10, the thruster firing is assumed to terminate when the vehicle first touches down, thus predicting the velocity of first impact. In Fig. 10, we see that the ground effects anticipated by this analysis essentially increase the ignition altitude that gives a minimal landing velocity. From Fig. 10, we also see that the change in impulse due to ground effects is a function of ignition altitude and has a maximum effect near for the optimal ignition altitude. Referring to Figs. 8–10, the increase in optimal ignition altitude for the ground-effects case is

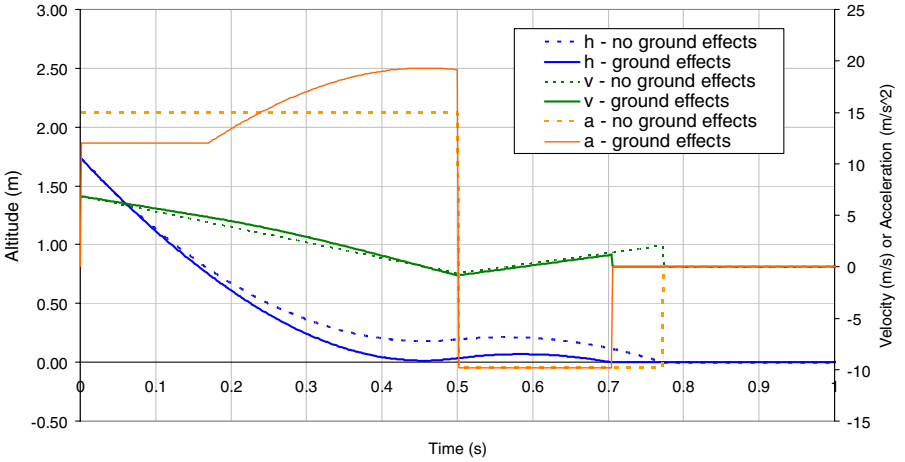

Fig. 8 Example CEV descent altitude h, velocity v, and acceleration a with and without ground effects for an ignition height of 1.74 m.

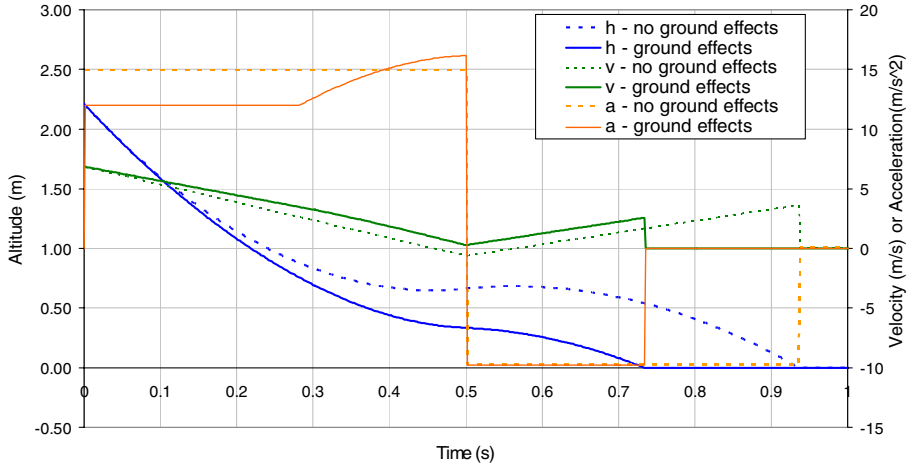

Fig. 9 Example CEV descent altitude h, velocity v, and acceleration a with and without ground effects for an ignition height of 2.20 m.

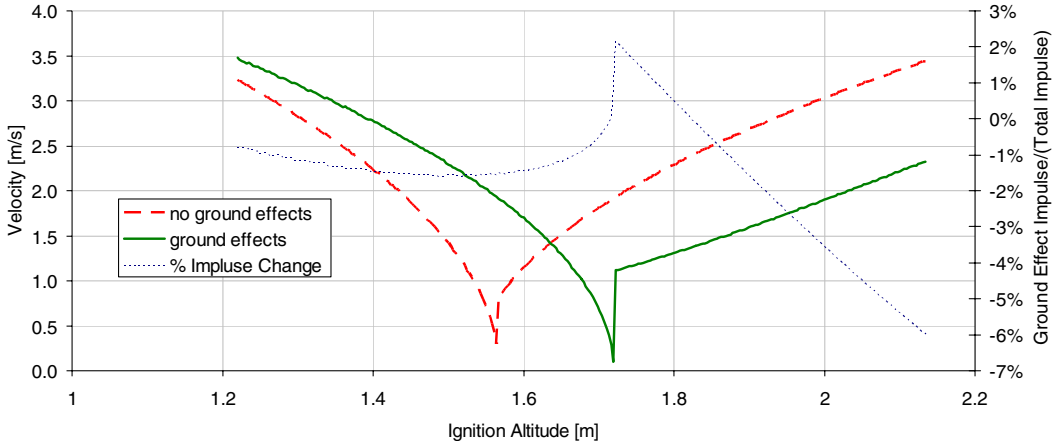

Fig. 10 Landing velocity as a function of ignition altitude, with and without ground effects. Also plotted is the percentage change of impulse due to ground effects.

due to the fact that ground effects generally cause thrust loss (except near the optimal firing height), which essentially increases the loss in height during thruster firing. Therefore, for ignition altitudes above the optimal, lower free-fall heights (the height at which the thrusters stop firing) are achieved by firing the thruster at higher altitudes than the no-ground-effects cases. For altitudes below the optimal (for the ground-effects curve in Fig. 10), ignition altitudes greater than the no-ground-effects cases are required, because the vehicle will otherwise hit the ground before the entire impulse of the thrusters is allowed to slow the descent velocity.

These results also show that the ground effects (under these assumptions) may serve to increase the range of desirable ignition altitudes for a maximum landing velocity requirement, thus increasing the error tolerance for ignition altitude. For example, Fig. 10 suggests that for a maximum landing velocity requirement of $\sim$1.5 m/s, the tolerable error for ignition altitude is $\pm$0.08 m if ground effects are ignored; however, if ground effects are taken into account, the tolerable error increases to $\pm$0.12 m. This flattening of the landing velocity curve in Fig. 10 due to ground effects can be understood by examining the relationships in Figs. 8 and 9. Essentially, if the ignition altitude is above the optimal value (when accounting for ground effects), the ground effects serve to cause a thrust loss that decreases the free-fall height with respect to the case without ground effects. On the other hand, if the ignition altitude is below the optimal value (again, when accounting for ground effects), the ground effects serve to provide a thrust gain just before impact that reduces the final landing velocity.

The advantage of the effects discussed previously is an increase in the tolerable error in ignition altitude; however, the disadvantage is that a detailed analysis, which includes ground effects, is required to determine the optimal ignition altitude. In conjunction with the preceding analysis, we also determined the change in attitude of the spacecraft due to the ground-effect-related torques given in Sec. II.A of this study. For the ignition altitudes from $\sim$1.2–2.44 m, the range of landing attitudes at impact is -0.66 to -5.8 deg about the y axis.

III. Conclusions

The results of this study show that ground effects can have a profound impact on landings performed with widely spaced supersonic retrorockets on a large flat surface. In particular, the results show that ground effects are extremely important for determining the final landing velocity and vehicle attitude for a CEV vertical retrorocket configuration. The steady-state results herein suggest that a CEV vertical retrorocket configuration will see a similar flowfield to that of subsonic multijet flows for V/STOL aircraft seen in earlier studies [2,6]. We also observe that thrust loss can increase due to the presence of the ground in the flowfield. The pressure drop increases in magnitude and area with decreasing altitude; however, the accompanying fountain upwash also increases in importance and eventually dominates and causes a thrust-gain effect at the lowest altitudes.

The dynamic analysis of CEV descent shows that the ground effects profoundly change the characteristics of the landing velocity of the CEV module. This is due to the fact that ground effects can impart a positive or negative change in total effective impulse, depending on the firing altitude. The analysis suggests that ground

effects increase the optimal ignition altitude and may serve to broaden tolerance for ignition altitude for a desired touchdown velocity. We identified scenarios that reflected the acceleration profile from the land-based Apollo drop tests; however, we did not see nearly as high a gain in impulse due to ground effects. The torque estimates due to ground effects cause a relatively small change in the vehicle attitude (i.e., several degrees); however, this effect may be important if considered with other possible torque sources, such as thrust imbalance.

The results discussed herein are estimated from steady-state conditions at a few altitudes to provide insight to a full transient analysis of the vehicle descent, and so more analysis is necessary to determine the actual ground effects. For future analyses, we plan to mimic the Apollo drop test with a full transient analysis to benchmark the model and our assumptions. Once we have verified our assumptions, we will do full transient analyses for the CEV design that will be used to assist Monte Carlo simulations of landing scenarios. We also intend to extend this analysis to include the horizontal retrorockets to determine the degree of the thrust loss for these rockets.

Acknowledgments

The research described in this study was funded by the Jet Propulsion Laboratory (JPL), California Institute of Technology, under contract with NASA. The authors would like to thank Joe Shepherd from the Graduate Aeronautics Laboratories at the California Institute of Technology (GALCIT); Colleen Marrese-Reading, Bob Frisbee, Ravi Prakash, and Josh St. Vaughn from JPL; and Jim Corliss from NASA Langley Research Center for their input into this study.

References

[1] Lands, J. F., "Development of a Terminal Landing Rocket System for Apollo-Type Vehicles," *Journal of Spacecraft and Rockets*, Vol. 4, No. 3, Mar. 1967, pp. 333–338. doi:10.2514/3.28862

[2] Kuhn, R. E., "Recommendations for Ground Effects Research for V/STOL and STOL Aircraft and Associated Equipment for Large Scale Testing," NASA CR-177429, Mar. 1986.

[3] Alvi, F. S., Ladd, J. A., and Bower, W. W., "Experimental and Computational Investigation of Supersonic Impinging Jets," *AIAA Journal*, Vol. 40, No. 4, Apr. 2002, pp. 599–609. doi:10.2514/2.1709

[4] Choutapalli, I. M., Krothapalli, A., Alkislar, M., and Lourenco, L., "Flowfield and Noise Characteristics of Twin Supersonic Impinging Jets," *AIAA Journal*, Vol. 45, No. 4, Apr. 2007, pp. 793–805. doi:10.2514/1.19914

[5] Krothapalli, A., Rajkuperan, E., Alvi, F., and Lourenco, L., "Flow Field and Noise Characteristics of a Supersonic Impinging Jet," *Journal of Fluid Mechanics*, Vol. 392, 1999, pp. 155–181. doi:10.1017/S0022112099005406

[6] Lummus, J. R., and Smith, E. W., "Flow Field Characteristics and the Effect of Jet-Exhaust Simulation for V/STOL Vehicles Near the Ground," *NADC V/STOL Aircraft Aerodynamics Symposium*, Naval Postgraduate School, Monterey, CA, 1979, pp. 293–313.

[7] Peroomian, O., Chakravarthy, S., Palaniswamy, S., and Goldberg, U., "Convergence Acceleration for Unified-Grid Formulation using Preconditioned Implicit Relaxation," AIAA Paper 1998-0116.

[8] Batten, P., Leschziner, M. A., and Goldberg, U. C., "Average-State Jacobians and Implicit Methods for Compressible and Turbulent Flows," *Journal of Computational Physics*, Vol. 137, No. 1, 1997, pp. 38–78. doi:10.1006/jcph.1997.5793

J. Martin
Associate Editor